NASA Technical Memorandum 105968
AIAA–93–0032

Results of Low Power Deicer Tests on a Swept Inlet Component in the NASA Lewis Icing Research Tunnel

Thomas H. Bond and Jaiwon Shin
Lewis Research Center
Cleveland, Ohio

Prepared for the
31st Aerospace Sciences Meeting & Exhibit
sponsored by the American Institute of Aeronautics and Astronautics
Reno, Nevada, January 11–14, 1993

NASA

RESULTS OF LOW POWER DEICER TESTS ON A SWEPT INLET COMPONENT IN THE NASA LEWIS ICING RESEARCH TUNNEL

Thomas H. Bond[+] and Jaiwon Shin[+]
National Aeronautics and Space Administration
Lewis Research Center, Cleveland Ohio

ABSTRACT

Tests were conducted under a USAF/NASA Low Power Deicer program on two expulsive technologies to examine system performance on hardware representative of a modern aircraft part. The BF Goodrich Electro-Expulsive Deicing System and Pneumatic Impulse Ice Protection System were installed on a swept, compound curve, engine inlet component with varying leading edge radius, and tested through a range of icing and system operating conditions in the NASA Lewis Icing Research Tunnel. A description of the experimental procedure and results, including residual ice thickness, shed ice particle size, and changes in system energy/pressure characteristics are presented here.

SYMBOLS AND ABBREVIATIONS

EEDS	Electro-Expulsive Deicing System
^{o}C	Centigrade
IRT	Icing Research Tunnel
LeRC	Lewis Research Center
LWC	Liquid Water Content, g/m^3
MVD	Median Volume Diameter, μm
NTSC	National Television Systems Committee
PAL	Phase Alternation Line
PEEK	Polyetheretherketone
PIIP	Pneumatic Impulse Ice Protection
PPS	pictures per second

INTRODUCTION

The United States Air Force (USAF) Materiel Command* and NASA have sponsored a joint program to examine the capabilities of advanced low power ice protection systems. The initial goal was to "freeze" the currently available technologies and assess their icing performance characteristics. This is reported in Refs.1 and 2. The tests also resulted in the development of new test methods and data acquisition systems to capture ice shedding events and quantify shed ice particle size [3]. Upon completion of this phase of the program, the USAF selected the BF Goodrich Electro-Expulsive Deicing System (EEDS) and the Pneumatic Impulse Ice Protection (PIIP) system to further test on a specific engine inlet application.

A component representative of an actual aircraft inlet part was chosen to test the two expulsive deicers under a range of operating conditions. This provided a rigorous installation and test environment that modelled an actual application.

Unlike conventional anti-icing systems, de-icing systems let ice accrete on the surface until there is enough mass to expel. The two deicing technologies mentioned above rely on very rapid surface displacement, induced by a repulsive force, to crack and debond the ice. Once expelled, the shed ice particles are carried away from the surface by the airflow. If an engine inlet or upstream airframe component is to be protected with these deicing systems, it must be designed so that shed ice particles are small enough not to damage the engine fan blades. The potential for future use of these systems on inlet applications will be determined in part by the size, shape, and number of particles that the engine can safely ingest.

This paper will discuss the experimental procedure used to conduct the test and present residual ice characteristics and shed ice particle size data.

TECHNICAL APPROACH

The model was tested under a range of icing and performance conditions to provide an array of variables for a parametric study. Both glaze and

---

[+] Aerospace Engineer, Member AIAA

* The program was originated with the USAF Air Logistics Center at Tinker Air Force Base, now a part of the Materiel Command

rime ice conditions were tested at a number of different temperatures. Deicer cycling time was varied, and operating pressure or capacitor bank energy was changed. Deicer system performance was measured by documenting residual ice thickness, photographic records, high speed imaging, and general notes on observational run sheets. Shed ice information was captured during each run on high speed videography and high speed 16 mm motion pictures. The data from the high speed videography was coupled to an image processing software package that resided on a workstation platform. This allowed the transfer of digitized visual information to a computer where the shed ice particle distributions and sizes were calculated through pixel identification and scaling techniques.

HARDWARE AND SYSTEM DESCRIPTION

Icing Research Tunnel

The NASA LeRC IRT is a closed-loop refrigerated wind tunnel. A 3728 kW (5000 hp) fan provides airspeeds up to 134 m/sec (300 mph). The refrigeration heat exchanger can control the total temperature from - 1.1 to - 42 ^{o}C. The spray nozzles provide droplet sizes from approximately 10 to 40 μm median volume droplet diameters (MVD) with liquid water contents (LWC) ranging from 0.2 to 3.0 g/m^{3}. The test section of the tunnel is 1.83 m (6 ft) high and 2.74 m (9 ft) wide.

Ice Protection Systems

The Pneumatic Impulse Ice Protection system was designed and developed by BF Goodrich [5] (Fig. 1). It uses pneumatic pressure to generate the ice debonding process. The deicer has a matrix of spanwise tubes imbedded in a composite leading edge. The tubes lay flat in the relaxed state. When the system is activated the rapid pressurization creates a shock wave which propagates longitudinally through the tube [6]. The tubes expand slightly with a resultant distortion of the outer surface that debonds the ice. The high acceleration of the skin due to the extremely fast pressure pulse launches the shattered ice particles into the airstream (Fig. 2). Polyetherether ketone (PEEK) was chosen from among many outer skin options for this test.

The BF Goodrich Electro-Expulsive Deicing System uses electro-magnetic repulsion to generate the forces necessary to shed ice. The deicer has multiple conductors (copper braids) cured in an elastomer nylon composite matrix [4]. A layer of teflon separates the upper and lower conductor sets (Fig. 3) that overlay each other. The conductors are designed such that the high amperage current pulse from a capacitor bank energy supply discharges through the overlaying sets in an opposing fashion, resulting in electro-magnetic fields that produce a repulsive force between the two layers. The bottom conductors are constrained by the outer surface of the airfoil, so the upper conductors move rapidly outward. This shatters the accreted ice and expels it outward. The elastomer matrix is the restoring force that returns the assembly to the relaxed position at the end of the deicing event.

Model Hardware

The test article chosen for this work was a swept, compound curve, engine inlet component with a varying leading edge radius (Fig. 4). The inlet section was 1.22 m (48 in) long with a sharp 90^{o} upper corner and a leading edge radius near the top of 6.35 mm (0.25 in). The section also had a sweeping lower curve with a leading edge radius near the bottom of 19.0 mm (0.75 in). The inlet section was centered vertically and attached to a generic afterbody that was bolted in the tunnel test section. Two large wooden plugs were fashioned to blend the top and bottom curves into the afterbody. They smoothed out the airflow to minimize the flow disturbances which might affect the ice accretions and the shed ice particles being expelled outward and downstream from the model.

The inlet section was connected to the afterbody with a hinged bracket that allowed quick removal of the inlet section. This was necessary to accommodate the two different deicers installed during the test. A swivel fixture was the second hardware point that secured the inlet section to the afterbody. This layout provided the latitude to adjust the angle-of-attack (AOA) of the inlet section without altering the centerline position of the afterbody. Once the AOA was set, the swivel plate was tightened to prevent movement.

Imaging Equipment

Three high speed videography systems were used. All were Kodak Ektapro 1000 Motion Analyzers. They consist of an intensified imager, controller, monitor, and the Ektapro 1000 Processor. The Kodak Ektapro 1000 Imager has a gated image intensifier assembly that functions as an electronic shutter and light amplifier. This increases the imager's ability to capture events in low light and reduces the blurring of objects moving rapidly through the field of view. The Intensified Imager Controller

sets the shutter and amplification functions. The intensified imager sends the video output to the Ektapro 1000 Processor where the image data is transferred to a special cassette tape that accepts magnetic media information at up to 1000 frames per second full field of view. The Processor can play back taped images, and set the communication protocols to transfer the visual information in video or digital format. Time, frame rate, session number, and other pertinent data are included in the transfer. The Ektapro 1000 Analyzer has a resolution of 240 columns of pixels by 192 rows of pixels, and provides a video output signal compatible with either NTSC (North American) standard or PAL (European) standard video recording signal formats.

The high speed 16 mm film camera was an NAC model E-10/EE. The camera was operated at 3000 pictures per second (PPS) and had a 122 m (400 ft) roll film magazine. This combination yielded 5 seconds of imaging data. Two black and white conventional video cameras were used for safety monitoring of the test and additional qualitative documentation. These data were recorded on S-VHS tapes. A 35 mm camera was used to record residual ice and other noteworthy ice accretion characteristics. A Sony Mavica 5000 still video camera was set up to have a field of view equivalent to the mid-span Ektapro coverage area. This provided a format readily adaptable to digitized image data to support the qualification of residual ice coverage.

TEST METHODS

Test Conditions

The ice protection systems were tested at one tunnel velocity over a range of temperatures and icing cloud conditions as outlined in Table 1. The conditions were chosen to cover both glaze and rime ice points at the highest tunnel airspeed obtainable with this model configuration. The icing spray times were varied between 10 and 16 minutes depending on the deicer cycling time. There were seven different cycling times: 15, 30, 60, 90, 120, 180, and 240 seconds. This provided ample points within the range to do an extensive examination of cycling time effects. From previous experience [1,2,3], the three primary cycling times targeted were 30, 60, and 90 seconds; the other times provided information to extend and define cycling time effects in the parametric study, and were not repeated as often. Two operating pressures, 4482 and 5516 kPa (650 and 800 psi), were used for the PIIP system, and three capacitor bank energy settings that resulted in peak electrical currents of 3300, 3550, and 4160 amperes were used for the EEDS.

Surface pressure was measured using a pressure belt to examine the angle-of-attack envelope for the 103 m/s airspeed by adjusting turntable angle. These data were used to provide the best possible setup configuration to obtain a pressure distribution similar to flight.

Test Procedure

A typical run was started by bringing the IRT to the desired operating condition and setting the spray bars for the appropriate LWC and MVD. Once the tunnel speed and temperature were stable, the video monitoring systems and deicer cycling control systems were initiated as the spray cloud was turned on. The deicer was actuated at the selected firing interval throughout the icing event, and one high speed imaging data point was taken during the spray as the deicer was fired. This yielded an image with a varied amount of obscurity depending on the LWC setting. At the end of the spray, before the final deicer firing, the tunnel was brought to idle and pre-fire information was documented. A still video pre-fire image of the ice was taken. As shown in Fig. 5, the ice on the inlet section was measured at seven locations using a modified dial indicator gage (Fig. 6). This provided a range of measurements for different leading edge radii, compound curve geometries at the top and bottom, and pressure side (lower surface) ice. Photographs were taken of the ice shapes, and general notes characterizing the ice were recorded. The frost was cleaned off the model aft of the impingement limits to improve the background contrast between the white shed ice particles and the black paint on the model. The tunnel was then brought up to speed and a second high speed imaging data point was taken during the final deicer firing. The tunnel was brought down to idle again, and a set of post-fire residual ice thickness measurements, photographs, and notes were recorded. A final still video image of the remaining ice was also acquired. The model was then cleaned off and prepared for the next icing test.

Visual Data Acquisition

Three Kodak Ektapro 1000 high speed video systems were used to collect information on ice shedding. Two were located in the IRT Control Room (Fig. 7) to monitor portions of the lower surface of the inlet section model. Image resolution was set to define a particle as small as 3.2 mm^2 (0.005 in^2) for post-test analysis requirements. The resulting dimensions for the fields of view were approximately 0.33 m (13 in) high and 0.41 m (15 in) wide for each camera. This small field of view is the result of severe

limitations imposed on the intensified imager camera resolution capabilities because of the high sampling rates, rapid shuttering, and low-light amplification. An NAC 16 mm high speed film camera was used as a backup system. Because of the better resolution of silver halide film, the field of view was substantially larger than the Ektapro camera field of view for an equivalent particle size requirement. All the high speed imaging data that has been reduced to date has been from the Ektapro systems. The sheer volume of image information collected during an ice shedding event, the fast processing capability, and the near real time data viewing of the high speed video system make it the primary tool for monitoring the shed ice events. The post-test processing routine for analyzing the data accommodates the digitized information format already available in the processor unit for the Ektapro high speed videography system. A complete shedding sequence can be automatically and quickly uploaded to the image processing package.

The final Ektapro system provided an overhead view of the lower surface area. This camera documented the ice that was expelled outward from the inlet section surface to provide information on how far the ice particles traveled away from the surface as they moved downstream. The data was used to apply a scaling factor for depth of field correction of the first two Ektapro Intensified Imager camera 2-D images.

Still images of both pre- and post-fire were taken to provide a visual record of the residual ice left on the inlet section. The leading edge and lower surface area just below mid-span were recorded with still video shots. It is intended to use this data to quantify residual ice coverage characteristics; however, the image processing software routine for this work is not completed yet. The 35 mm camera pictures and the standard video camera S-VHS tapes supplied a qualitative record of the system performance.

Deicer Imaging Setup

The imaging data for the shed ice events was recorded once during the spray, and once at the end of the run with the spray off. Each deicer cycle for both systems had multiple zone firings and the imaging equipment recorded every zone discharge during the shed event. Figures 8 and 9 show the zone layout, the deicer firing sequence, and the Ektapro fields of view for the PIIP and EEDS, respectively. In both cases, the lower curve area was viewed for the Zone 1 firing and the mid-span area for the Zone 2 discharge.

The EEDS had three separate zones approximaetly 0.43 m (17 in) long. Each zone was fired once, and since the coverage area wrapped around the leading edge to the upper surface, there was only a single shed event per deicer firing cycle in the Ektapro camera fields of view. The PIIP system setup substantially complicated the task of capturing the full set of shed ice data. There were two spanwise zones which split at the leading edge, and each zone was fired 1/4 second apart, then refired 3 seconds later. Thus, the camera fields of view recorded shed ice four times for every deicer firing cycle. The upper surface zone expelled ice off the leading edge and somewhat into the adjacent coverage area every time it was fired, meaning ice particles were carried past the lower surface field of view. The lower surface zone was directly in the field of view.

Image Processing

A new test technique using image processing has recently been developed to automate the process of analyzing shed ice events [3]. The package works on a UNIX based operating system on a Silicon Graphics Incorporated (SGI) workstation. For this test, the program received digitized images through an IEEE input port (Fig. 10), stored the information as picture files, and provided a number of image processing choices to analyze the data.

After up-loading the high speed imaging data to the SGI workstation, the image of the shedding event is reviewed from the pre-shed condition (Fig.11) throughout the ice shedding event. Figure 12 is a typical image of ice being expelled off the inlet section. The typical number of images analyzed is 25 to 40 frames, with each frame capturing 1 millisecond of the ice shed event. When all the shed ice has left the field-of-view, the last image is selected as a static background image and it is subtracted from all the frames for that particular ice shedding session. This leaves only the actual ice shed off the model as the event is replayed (Fig. 13). A grey level (tonal contrast from white through grey to black) within an ice particle is selected as a threshold value, then all the pixels with higher grey levels than the threshold value become pure white and the rest become pure black background (Fig. 14). One or several frames of this shed ice event can now have the ice particle size(s) measured. To do this, each particle in the image field has the number of pixels within its boundary counted, then a scaling factor is applied to convert these values to areas.

The program provides a tabular output of the shed ice particle size distribution from the frames

selected, and can plot this out in particle count versus the size distribution. This plot contains all the ice particle sizes tabulated from each processed image frame. This means an individual ice shed particle will be counted as many times as it appears in consecutive frames of the shed event. By drawing an upper bound curve on the plot along the outer perimeter of the shed ice particle size distribution, the data now represents a worst case condition for that run (Fig. 15). Ice particles within a given frame can also be selected individually and have an area value calculated.

It should be noted that the lower right-hand tail of the curve (Fig. 15, boxed in area) is not always an accurate indication of the largest particle sizes. There are two image processing effects happening here that can provide ambiguous results. First, this boxed area may contain particles that are overlapped in the 2-D image plane and are counted as one large particle. Second, the number of frames examined usually includes some near the very beginning of the ice shed event where the large ice particles are not all completely broken up into their steady state sizes by the airloads. This also yields ice particles that are too large. Both anomalies should be considered during the data analysis; making individual measurements for the largest particles using the single particle measurement menu of the image processing routine will help screen out these potential errors and confirm the accuracy of this region of the plot.

The shed ice data from both expulsive deicers was catalogued and reduced in a similar fashion. The imaging frames that contained the shed ice event were saved and then analyzed for the ice particle size distribution and the largest particle sizes. Each shed event was reviewed by scanning through all the frames where the ice was expelled off the inlet section surface and carried aft by the airstream. At this time, the biggest 2 or 3 ice particles were chosen from the frames where they presented their largest frontal view. The area was then calculated in the image processing package. This scanning process also allowed the reviewer to define the start and end frames of the image set for particle size distribution data. Selecting the end point is straightforward - when the ice particles have left the field of view the shed event is over. Choosing the beginning point is more difficult; a compromise frame was picked where the large particles appear to be broken into their steady state size by the airloads, but the smaller particles were not so far downstream that many of them have left the camera field of view. Once these two end points were defined the image processing package identified and calculated the size of each ice particle in every frame and arrayed the data in a tabular format.

Energy/Pressure Measurements

The energy settings for the EEDS system were monitored on a selected basis by capturing the capacitor bank discharge traces for both current and voltage on a Hewlett Packard HP 5450 1A Digital Storage Scope. The device was equipped with a printer for hard copy output. This provided amperage and voltage traces to determine peak values and current rise time. The operating pressure for the PIIP system was hand recorded from a pressure gage located downstream of the regulator but in front of the impulse valve. The effects from the change in energy and operating pressure values are examined in the results section.

RESULTS

Documentation for the icing encounter can be divided into two broad categories. First, the shed ice particle size is important when examining conditions that are pertinent to engine ice ingestion or mechanical damage on downstream aircraft components. Second, the distribution, texture, quantity, and thickness of ice remaining on a surface have a direct relation to aero-performance concerns. However, during these tests residual ice characterization was limited to thickness measurements. The results section will cover only mid-span measurements of the residual ice thickness and selected shed ice particle size results. The large volume of data for both measurements across the span of the model for different power and pressure settings, through a range of cycling time, icing, and temperature conditions, makes it unrealistic to present the full results of a parametric study for both deicers in this paper.

Residual Ice Data

The residual ice thickness measurement results for model mid-span are listed for the PIIP system in Table 2, and the EEDS in Table 3. Both pre- and post-fire data points are included to provide the bounds for deicer ice removal performance. During normal deicing operations, the pre-fire condition represents the worst residual ice characteristics the inlet section will encounter, and the post-fire condition represents the minimum thickness of residual ice on the inlet surface. The values in Tables 2 and 3 for each condition at both the leading edge and lower surface are the average of all the repeat runs (up to three) at that point. For most test points, the repeat values were very similar; however, there were occasions when the ice thickness measurements varied by as much as 50 to 60%.

These were usually at the low cycling times where there tended to be more data scatter in general; the measurements for cycling times of 60 seconds and above were more repeatable (usually less than 20% variability). The plots in Figs. 16 through 19 are of the residual ice characteristics at the mid-span of the model. The PIIP system measurements in these plots and Table 2 for the leading edge and lower surface were taken at points 3 and 4, respectively, in Fig. 5(b). The EEDS data for these figures and Table 3 are based on ice thickness measurements at the leading edge and lower surface taken at points 2 and 3, respectively, in Fig. 5(a). The lower input pressure for the PIIP system, and the mid-power for the EEDS, were the baseline configurations set by BF Goodrich, and the plots in Fig. 16 through 19 used these settings.

Figures 16 and 17 show residual ice thickness measurements for both systems at -2.2° C, a warm glaze ice condition. The post-fire data show that the PIIP system cleaned the ice off the leading edge completely and the EEDS performed equally well above the 30 second cycling time. Both systems consistently left less than 0.5 mm of ice on the lower surface for this temperature.

Figures 18 and 19 are of the measured ice thickness for a rime condition at -20° C. At the leading edge, the ice removal for both systems was very similar. The deicers cleared the ice off the mid-span of the inlet component for cycling times of 60 seconds and above; for 15 and 30 seconds cycling times, ice remained on the surface of the leading edge. The lower surface ice removal performance for the rime condition proved more challenging than the equivalent glaze ice condition. The PIIP system did not clear the ice off the surface until the 90 second firing cycle, and the EEDS had residual ice throughout the cycling interval range. However, the thickness left in these cases was about 0.6 mm or less. This was deemed to be an insignificant amount for this application, but may not be for other configurations where even very small amounts of surface roughness result in a large aerodynamic penalty.

A more in-depth examination of the residual ice results from this work and another USAF/NASA test can be found in Ref. 7.

Shed Ice Data

Although imaging data of the shed ice event were recorded twice during the spray, the imaging records were usually analyzed from the data set at the end of the run where there was no spray cloud obscurity. Most test conditions have two or three repeat test points where data were recorded and analyzed. This allowed the examination of repeatability within a subset of conditions. For this IRT entry, operating pressure/energy (for PIIP/EEDS), temperature, or cycling time were varied independently while the other parameters were held constant. Along with this, there were two separate viewing sights on the model to categorize geometry effects. The particle distribution effects discussed in this paper were based on a choice of a sample set of the data from the total matrix of variables.

Single Ice Particle Size Measurements

The single particle area data for the deicers can be found in Tables 4 and 5. Each one of the values in the tables is the largest particle size that was individually measured by the image processing routine. The tables include both the mid-span and lower curve views of the deicers as shown in Figs. 8 and 9. In the examination of these data to date, few consistent trends have been found. In the PIIP system (Table 4), the mid-span data for the warmest three temperatures does show an increase in size with the longer cycling times, but that trend is not evident for the lower curve area. There is some agreement for the EEDS (Table 5) with the above trend, but it is not repeated for every temperature. There is a fair amount of scatter in these single particle size measurements; however, these data can be used to determine the largest ice particle released during a shed event for this test configuration.

Ice Particle Size Distribution Measurements

The repeatability of the data is the basis for the confidence associated with the trends of the parameter study. A series of plots were generated to examine repeatablility; Fig. 20 is typical of the repeatability for the mid-span location for both systems with a 60 second firing cycle. The repeatability of the higher cycling times was equivalent to that shown; however, the 15 and 30 second cycling times and some of the inlet section lower curve plots had slightly poorer repeatability.

The rest of the trends detailed here for the shed ice distribution data will only deal with 30, 60, and 90 second cycling times. These values were the primary cycling intervals for the test and highlighting their characteristics will keep the results to a manageable data set. The plots are also based on the lower pressure setting for PIIP, and the mid-power energy setting for EEDS unless otherwise noted.

The temperature and LWC effects were combined because the nature of this test did not allow the expansion of the test matrix to change one independent variable at a time. The LWC varied from 0.70 down to 0.38 g/m^3 for the primary test temperatures of -2.2° to -20° C. Although limited work was done at two different LWC settings at -24° C, there were not enough repeat runs to confirm any trend at even this one temperature setting. Figure 21 indicates there is no effect for these combined parameters on ice particle distribution results. It is reasonable to assume that the high accelerations initiated by both these expulsive deicers to remove the ice are so great that these temperature/LWC settings are unimportant.

The lower curve of the engine inlet component has a large leading edge radius and a wide sweeping concave curve on the inner surface that provides a substantially different geometry from the mid-span region. The difference in shed ice particle distribution performance between the two sites was just as noticeable. As shown in Fig. 22, ice shed from the mid-span was larger and farther out on the tail end of the curve than that shed from the lower lip.

The changes in input settings for energy and pressure for the two deicers had only a marginal effect on the outer bound curve of the shed ice distribution. Figure 23 for the EEDS is typical of the results encountered for energy/pressure setting differences.

Figure 24 reinforces the results found in previous tests when altering the deicer cycling time. The cycling times of 60 and 90 seconds have curves that overlay each other or are very close together, while the curve for the cycling time of 30 seconds shows much smaller particles. The performance of these deicer systems is related to a threshold ice thickness. As the cycling time increases there is thicker ice on the deicer between firings. At some threshold value between 30 and 60 second cycling times, there is a definable break between ice particle size distribution profiles. For the higher cycling times, the distribution curves are quite similar, but the largest ice particle sizes grow with cycling time. This implies that there may be a threshold ice thickness below which the ice particles could be more easily broken up into smaller sizes.

Although both deicers are expulsive systems, they have different ice removal characteristics based on the deicer discharge which creates the dynamic mechanical properties that break the ice-to-surface adhesion. In comparing the ice particle size distribution data for the two deicer systems, the PIIP system has smaller size distribution curves than the EEDS. Figure 25 supports this observation and also includes an equivalent difference in large end particle sizes between the two systems. It should be noted that the difference has been quantified only for this specific inlet section configuration, and cannot be generalized for all applications.

Table 6 summarizes the effects for both deicers discussed for Figs. 21 through 25. The outer bound shed ice curves for the ice particle size distribution at the largest size end of the plot showed some different characteristics than the main body of the distribution curves. Table 7 lists these results separately for the same trends as in Table 6. These data have to be viewed with the qualifications discussed at the end of the Image Processing section on page 4.

CONCLUDING REMARKS

This joint USAF/NASA program provided the opportunity to characterize the performance of two new low power impulse type deicers by examining the ice expulsion process. An extensive database including variations in energy and operating pressure, and a range of cycling times, temperatures, and icing conditions provided the basis for a detailed parametric study of both residual ice and shed ice information. These tests, conducted on the complex, compound geometry of an engine inlet component, allowed the analysis of the shed ice particle size distribution for support of engine fan blade Foreign Object Damage considerations.

Although PIIP performance was slightly better then EEDS for the data analyzed, neither system had been optimized for the complex geometry tested. The results shown on this complex shape are very encouraging; however, further work is needed to optimize the deicing system operating and performance characteristics for this type of geometry.

REFERENCES

1. Bond, T.H., Shin, J., and Mesander, G.A., "Advanced Ice Protection Systems Test in the NASA Lewis Icing Research Tunnel," NASA TM 103757, Presented at 47th Annual American Helicopter Society Forum and Technology Display, Phoenix, AZ, May, 1991.

2. Bond, T.H., Shin, J., Mesander, G.A., and Yeoman, K.E., "Results of USAF/NASA Low Power Ice Protection Systems Test in the NASA Lewis Icing Research Tunnel," NASA TP-3319, 1992.

3. Shin, J., Bond, T.H., and Mesander, G.A.,"Results of a Low Power Ice Protection System Test and a New Method of Imaging Data Analysis," NASA TM 105745, Presented at 48th Annual American Helicopter Society Forum and Technology Display, Washington, D.C., June, 1992.

4. Byrd, D., "Electro-Expulsive Deicing System & Compound Curve Surface Applications," Proceedings of the SAE/AHS Aircraft Icing Technology Workshop, Cleveland, Ohio, September, 1992.

5. Martin, C. and Putt, J.C.,"An Advanced Pneumatic Impulse Ice Protection System (PIIP) for Aircraft," AIAA Paper 90-0492, January 1990.

6. Putt, J.C., "Current Pneumatic Impulse Ice Protection (PIIP) development Status," Proceedings of the SAE/AHS Aircraft Icing Technology Workshop, Cleveland, Ohio, September, 1992.

7. Shin, J., and Bond, T.H., "Surface Roughness Due To Residual Ice In The Use Of Low Power Deicing Systems," AIAA Paper 93-0031, January, 1993.

Table 1
IRT Test Conditions

Airspeed m/s / mph	T_{total} ^{o}C / ^{o}F	LWC g/m^3	MVD μm
103 / 230	-2.2 / 28.0	0.70	20
103 / 230	-6.7 / 20.0	0.50	20
103 / 230	-20.0 / -4.0	0.38	20
103 / 230	-23.9 / -11.0	0.38	20
103 / 230	-23.9 / -11.0	1.00	20

Table 2

Residual ice on leading edge and lower surface at mid-span for BF Goodrich PIIP (Fig. 5 (b), points 3 & 4 on the PIIP model)
Ice thickness measurement values are the average of all repeat runs for a data point

Leading Edge Data (point 3) in mm

Cycle Time (sec)	4482 kPa input operating pressure T_{total} (°C) / LWC (g/m^3)										5516 kPa input operating pressure T_{total} (°C) / LWC (g/m^3)									
	-2.2°/0.70		-6.7°/0.50		-20°/0.38		-24°/0.38		-24°/1.00		-2.2°/0.70		-6.7°/0.50		-20°/0.38		-24°/0.38		-24°/1.00	
	Pre	Post	Pre	Post	Pre	Post	Pre	Post	Pre	Post	Pre	Post	Pre	Post	Pre	Post	Pre	Post	Pre	Post
15	1.45	~	1.09	0.46	0.58	0.23	0.41	0.30	0.63	~	1.34	~	0.66	0.43	0.53	0.25	0.66	0.53	1.24	~
30	1.42	~	1.02	0.48	0.76	0.53	0.71	0.33	1.73	~	1.19	~	1.32	~	1.04	~	1.09	~	1.98	~
60	2.23	~	2.16	~	1.68	~	1.70	~	2.72	~	2.54	~	2.36	~	1.65	~	1.75	~	4.11	~
90	3.73	~	3.12	~	2.39	~					3.68	~	3.45	~	2.49	~				
120	5.25	~	3.81	~	2.87	~					3.86	~	4.44	~	3.56	~				

~ none or negligible
pre measurement taken prior to the final deicer firing - this case has the thickest ice on the airfoil surface during operation
post measurement taken after the final deicer firing - this case has the least amount of ice on the airfoil surface during operation

Lower Surface Data (point 4) in mm

Cycle Time (sec)	4482 kPa input operating pressure T_{total} (°C) / LWC (g/m^3)										5516 kPa input operating pressure T_{total} (°C) / LWC (g/m^3)									
	-2.2°/0.70		-6.7°/0.50		-20°/0.38		-24°/0.38		-24°/1.00		-2.2°/0.70		-6.7°/0.50		-20°/0.38		-24°/0.38		-24°/1.00	
	Pre	Post	Pre	Post	Pre	Post	Pre	Post	Pre	Post	Pre	Post	Pre	Post	Pre	Post	Pre	Post	Pre	Post
15	1.35	0.51	0.68	0.33	0.56	0.35	0.30	0.25	0.56	~	1.17	0.43	0.38	0.30	0.30	0.28	0.41	0.28	0.43	0.23
30	1.70	0.38	1.07	0.41	0.63	0.28	0.41	0.25	0.81	~	1.62	0.30	0.76	0.28	0.71	0.33	0.43	0.43	0.94	0.23
60	2.82	0.15	1.34	0.25	0.99	0.51	0.86	~	1.70	~	2.92	0.18	1.14	0.23	0.76	0.48	0.84	0.28	1.57	0.51
90	4.52	0.25	2.06	0.35	1.19	~					4.44	0.43	1.98	0.18	1.09	0.43				
120	6.35	0.38	2.64	0.18	1.47	~					6.30	~	2.74	~	1.57	0.30				

~ none or negligible
pre measurement taken prior to the final deicer firing - this case has the thickest ice on the airfoil surface during operation
post measurement taken after the final deicer firing - this case has the least amount of ice on the airfoil surface during operation

Table 3

Residual ice on leading edge and lower surface at mid-span for BF Goodrich EEDS (Fig. 5 (a), points 2 & 3 on the EEDS model)
Ice thickness measurement values are the average of all repeat runs for a data point

Leading Edge Data (point 2) in mm

Cycle Time (sec)	low power (3300A) T_{total} (°C) / LWC (g/m^3)				mid-power (3550A) T_{total} (°C) / LWC (g/m^3)						high power (4160A) T_{total} (°C) / LWC (g/m^3)									
	-6.7°/0.50		-20°/0.38		-2.2°/0.70		-6.7°/0.50		-20°/0.38		-2.2°/0.70		-6.7°/0.50		-20°/0.38		-24°/0.38		-24°/1.00	
	Pre	Post	Pre	Post	Pre	Post	Pre	Post	Pre	Post	Pre	Post	Pre	Post	Pre	Post	Pre	Post	Pre	Post
15	1.73	1.30	0.99	~	1.29	0.71	1.75	1.32	1.14	0.79	1.07	~	1.17	0.89	0.94	0.71	1.14	0.13	0.94	0.91
30	3.00	1.75	*		1.29	0.76	1.50	0.86	1.65	0.25	1.45	~	1.02	0.38	1.02	0.30	1.45	~	2.16	~
60	3.10	1.63	2.31	~	2.44	~	2.51	1.57	2.16	~	2.16	~	2.54	~	2.13	~	2.21	~	4.65	~
90	*		*		2.11	~	2.67	~	2.44	~	1.93	~	2.41	~	2.13	~				
120	3.17	~	2.36	~	2.67	~	3.00	~	2.79	~	2.64	~	2.92	~	2.46	~				

~ none or negligible * no data
pre measurement taken prior to the final deicer firing - this case has the thickest ice on the airfoil surface during operation
post measurement taken after the final deicer firing - this case has the least amount of ice on the airfoil surface during operation

Lower Surface Data (point 3) in mm

Cycle Time (sec)	low power (3300A) T_{total} (°C) / LWC (g/m^3)				mid-power (3550A) T_{total} (°C) / LWC (g/m^3)						high power (4160A) T_{total} (°C) / LWC (g/m^3)									
	-6.7°/0.50		-20°/0.38		-2.2°/0.70		-6.7°/0.50		-20°/0.38		-2.2°/0.70		-6.7°/0.50		-20°/0.38		-24°/0.38		-24°/1.00	
	Pre	Post	Pre	Post	Pre	Post	Pre	Post	Pre	Post	Pre	Post	Pre	Post	Pre	Post	Pre	Post	Pre	Post
15	1.44	0.53	0.76	0.66	2.01	0.53	1.07	0.63	0.86	0.51	2.03	0.25	0.79	0.79	0.68	0.53	0.89	0.51	0.76	0.48
30	1.75	0.86	*		2.06	0.38	0.99	0.56	0.96	0.58	2.16	0.33	1.04	0.53	0.76	0.58	0.91	0.53	1.57	0.48
60	1.98	0.58	1.73	0.79	2.90	0.36	1.32	0.58	1.22	0.79	3.73	0.38	1.93	0.51	1.19	0.46	0.96	0.46	2.29	0.46
90	*		*		4.27	0.25	1.83	0.48	1.68	0.66	4.19	0.28	1.60	0.51	1.17	0.89				
120	1.90	0.74	2.16	0.76	4.75	0.38	2.72	0.56	1.12	0.61	5.94	0.23	2.21	1.12	1.12	0.53				

~ none or negligible * no data
pre measurement taken prior to the final deicer firing - this case has the thickest ice on the airfoil surface during operation
post measurement taken after the final deicer firing - this case has the least amount of ice on the airfoil surface during operation

Table 4

Shed ice particle size measurement for single particles on the BF Goodrich PIIP System
Values are for the largest particle size of all deicer firings for a test condition, in cm^2

Cycle Time (sec)	4482 kPa input operating pressure T_{total} (°C) / LWC (g/m^3)										5516 kPa input operating pressure T_{total} (°C) / LWC (g/m^3)									
	-2.2°/0.70		-6.7°/0.50		-20°/0.38		-24°/0.38		-24°/1.00		-2.2°/0.70		-6.7°/0.50		-20°/0.38		-24°/0.38		-24°/1.00	
	LC	MS	LC	MS	LC	MS	LC	MS	LC	MS	LC	MS	LC	MS	LC	MS	LC	MS	LC	MS
15	2.480	0.554	0.304	1.090	0.535	0.950	0.357	0.339	0.701	0.984	1.476	0.554	3.173	0.241	2.305	0.403	0.512	0.225	1.719	2.298
30	0.703	1.270	0.643	0.772	1.536	0.823	0.736	1.032	0.773	2.008	1.403	0.661	1.434	0.613	1.250	0.821	0.368	0.628	3.683	1.706
60	1.204	0.978	0.964	1.129	1.143	1.154	1.102	0.628	1.537	2.245	0.666	1.645	1.333	0.952	3.090	1.628	1.948	1.517	1.897	0.712
90	0.786	1.124	0.886	1.419	0.864	2.248					1.016	1.965		2.226	3.229	2.012				
120	1.381	1.627	1.182	2.056	1.879	2.152					0.816	1.812	3.000	2.838	1.040	2.385				

LC lower curve of movable lip model, Ektapro #1 view in Figure 8
MS mid-span of movable lip model, Ektapro #2 view in Figure 8

Table 5

Shed ice particle size measurement for single particles on the BF Goodrich EEDS
Values are for the largest particle size of all deicer firings for a test condition, in cm^2

Cycle Time (sec)	low power (3300A) T_{total} (°C) / LWC (g/m^3)				mid-power (3550A) T_{total} (°C) / LWC (g/m^3)						high power (4160A) T_{total} (°C) / LWC (g/m^3)									
	-6.7°/0.50		-20°/0.38		-2.2°/0.70		-6.7°/0.50		-20°/0.38		-2.2°/0.70		-6.7°/0.50		-20°/0.38		-24°/0.38		-24°/1.00	
	LC	MS	LC	MS	LC	MS	LC	MS	LC	MS	LC	MS	LC	MS	LC	MS	LC	MS	LC	MS
15	1.074	0.974	1.051	1.812	1.191	0.637	2.792	0.947	2.541	1.577	0.530	0.474	1.040	1.325	1.043	1.048	1.035	0.688	2.275	
30	0.790	0.724	1.055	1.094	0.690	1.208	1.121	1.381	1.757	1.899	1.027	1.043	2.895	2.046	0.835	1.063	1.016	0.821	1.169	
60	1.516	4.249	0.770	3.074	1.500	2.452	1.557	1.770	1.630	3.155	0.936	0.773	2.930	2.414	2.856	1.384	1.104	1.313	1.434	
90					2.548	2.059	1.595	1.778	2.310	2.164	1.012	1.094	2.401	1.476	1.332	1.223				
120	0.899	3.396	2.328	4.344	1.726	3.493	2.019	1.946	2.087	3.218	0.803	1.744	3.943	0.968	1.509	2.639				

LC lower curve of movable lip model, Ektapro #1 view in Figure 9
MS mid-span of movable lip model, Ektapro #2 view in Figure 9

Table 6
Effect of Test Parameters on Shed Ice Particle Size Distribution

Parameters	Effects on Particle Size Upper Bound Curve
Cycling Time	yes (30 sec<60 sec ≈ 90 sec)
Temperature/ LWC	no
Geometry	yes (lower lip<mid-span)
Energy/Input Pressure	marginal
System Comparison	PIIP<EEDS

Table 7
Effect of Test Parameters on Maximum Shed Ice Particle Size in Distribution

Parameters	Effects on Larger Particles of the Distribution Curves
Cycling Time	no trend
Temperature/ LWC	EEDS: no trend PIIP: lower lip<mid-span
Geometry	no trend
Energy/Input Pressure	EEDS: high<mid<low PIIP: mid<high
System Comparison	PIIP<EEDS

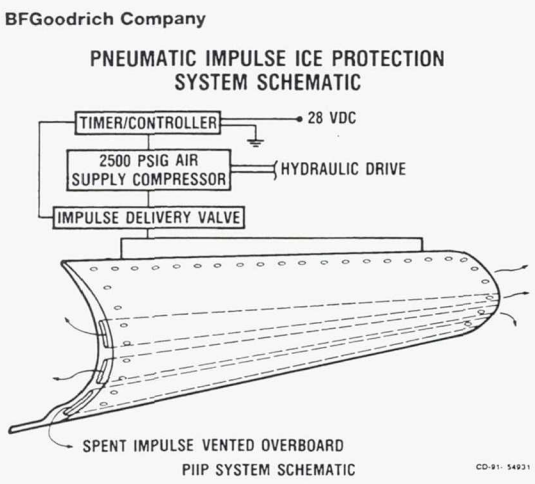

Figure 1. BF Goodrich Pneumatic Impulse Ice Protection (PIIP) System Schematic

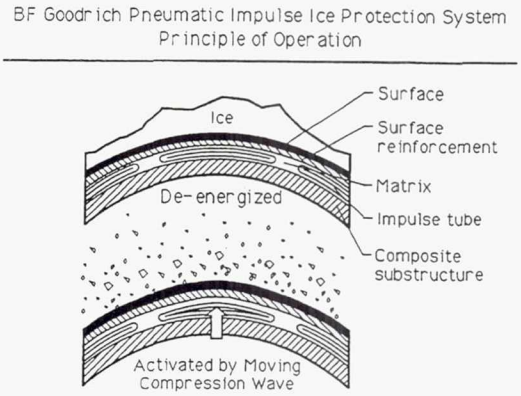

Figure 2. BF Goodrich PIIP System in Operation

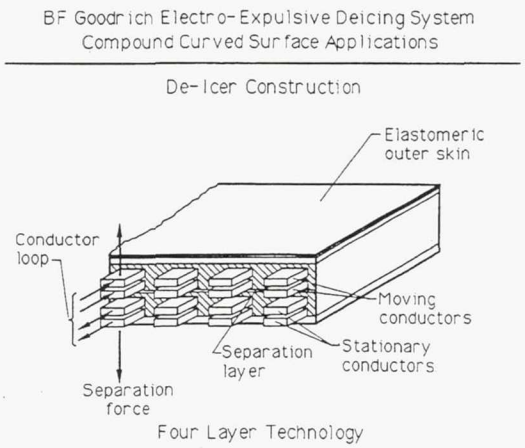

Figure 3. BF Goodrich Electro-Expulsive Deicing System (EEDS) Schematic

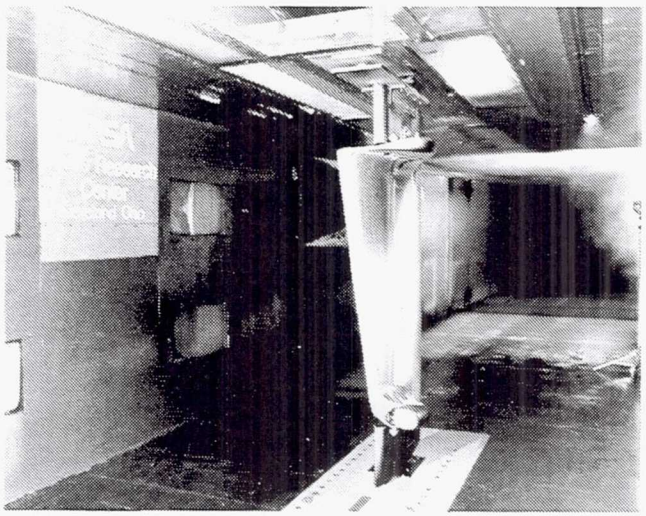

Figure 4. Engine Inlet Component With Generic Afterbody in NASA LeRC IRT

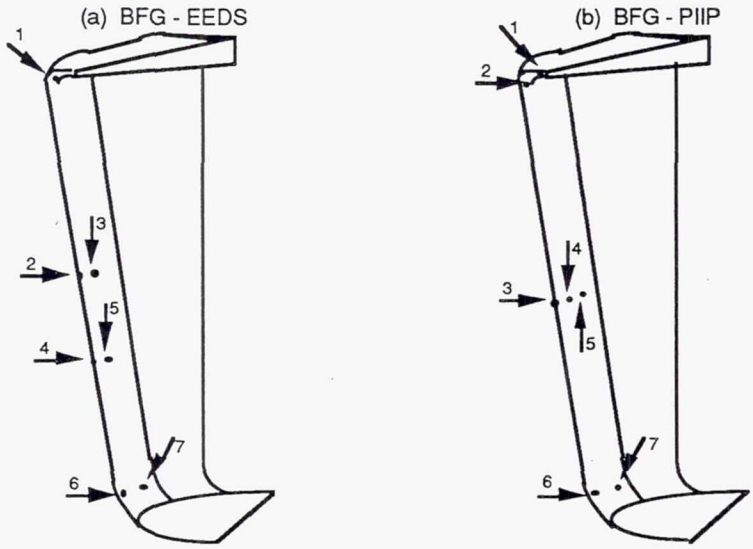

Figure 5. Residual Ice Measurement Locations for Both Deicers

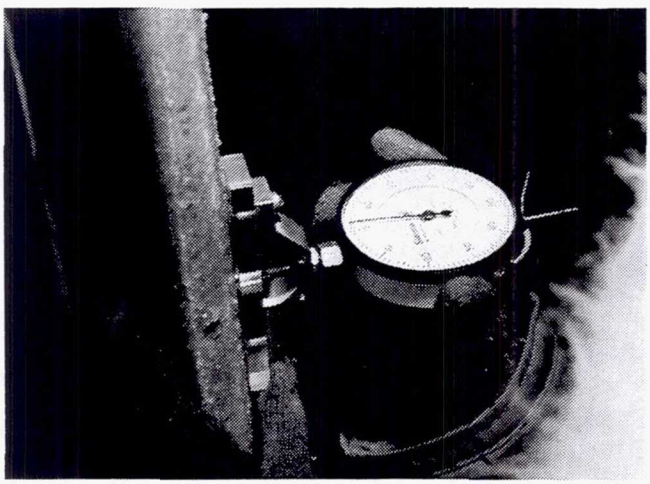

Figure 6. Lower Surface Ice Thickness Measurement

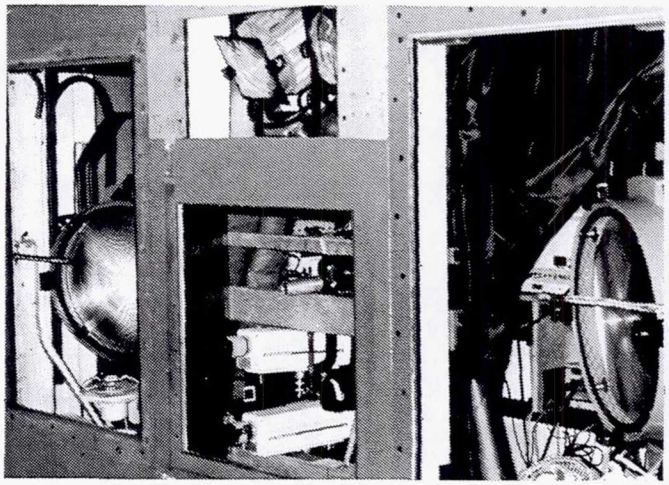

Figure 7. High Speed Videography Cameras in IRT Control Room

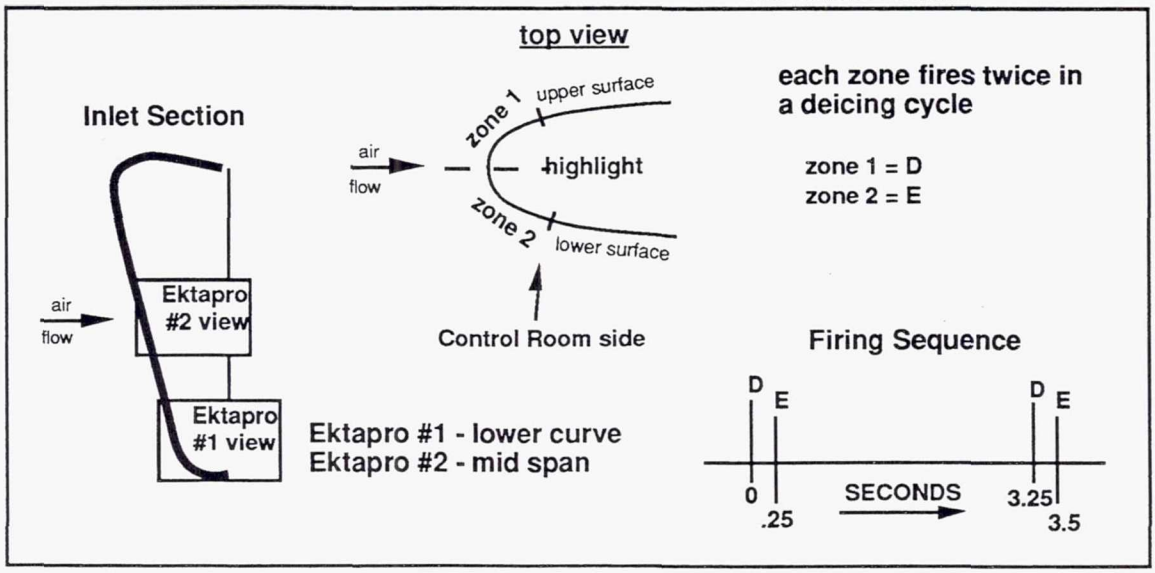

Figure 8. Deicer Zone and Imaging Equipment Layout for BFGoodrich PIIP

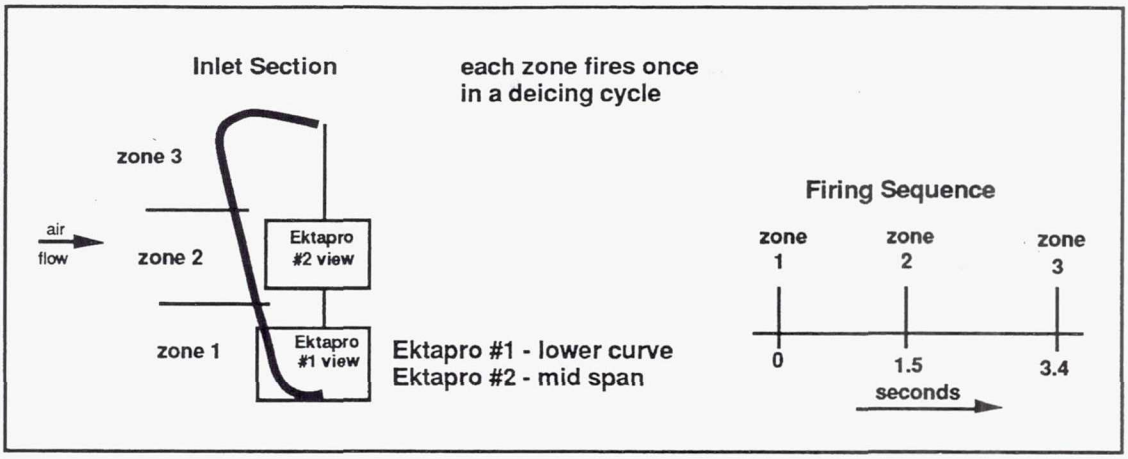

Figure 9. Deicer Zone and Imaging Equipment Layout for BFGoodrich EEDS

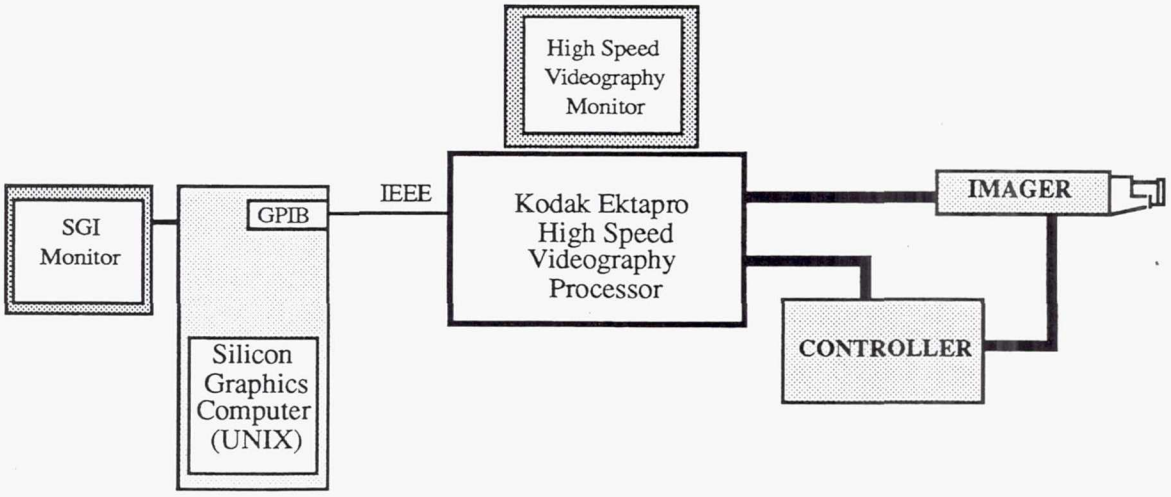

Figure 10. Schematic View of High Speed Videography and Image Processing Systems

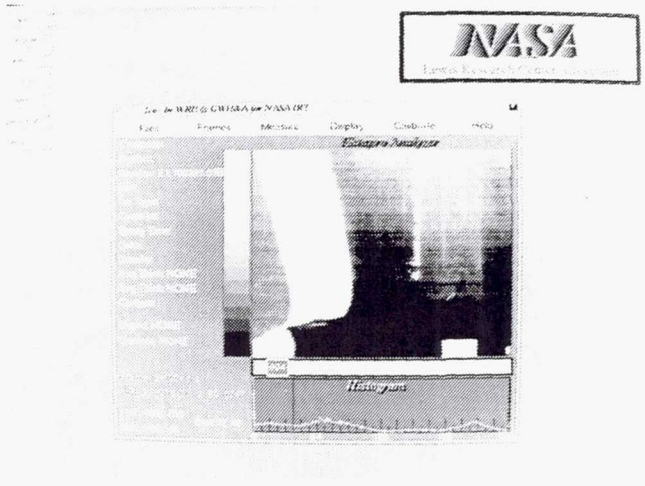

Figure 11. Image Processing Routine - Pre-shed Condition

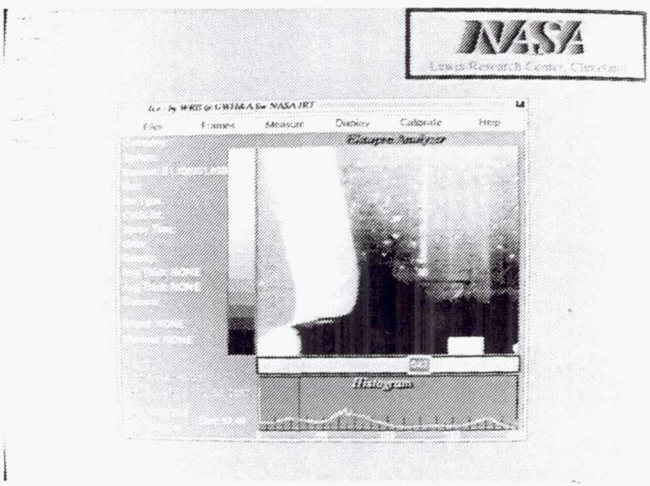

Figure 12. Image Processing Routine - During Ice Shedding Event

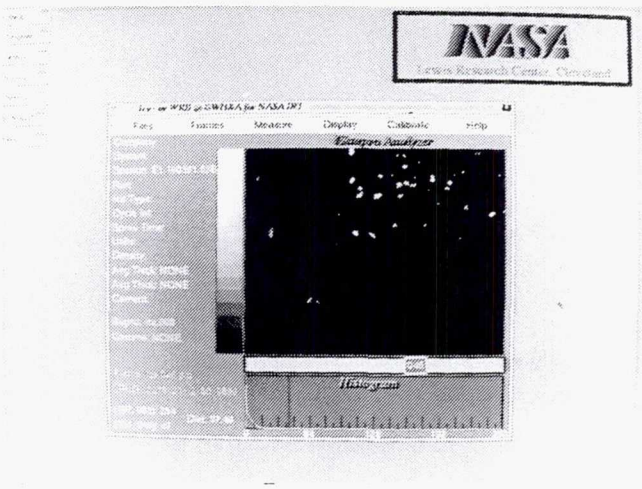

Figure 13. Image Processing Routine - After Image Subtraction

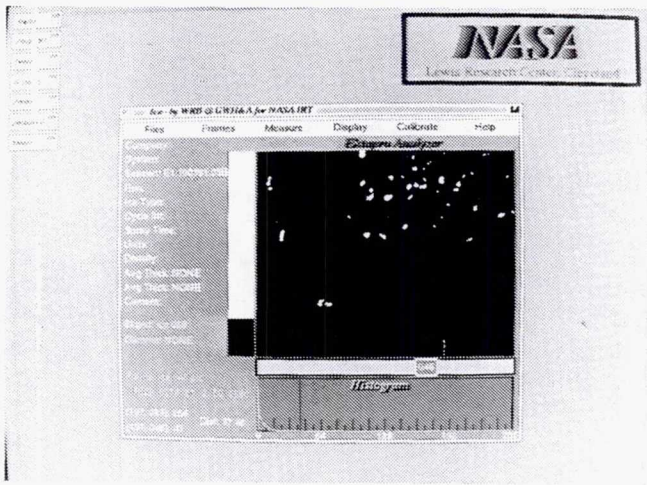

Figure 14. Image Processing Routine - After Grey Scale Threshold is Set

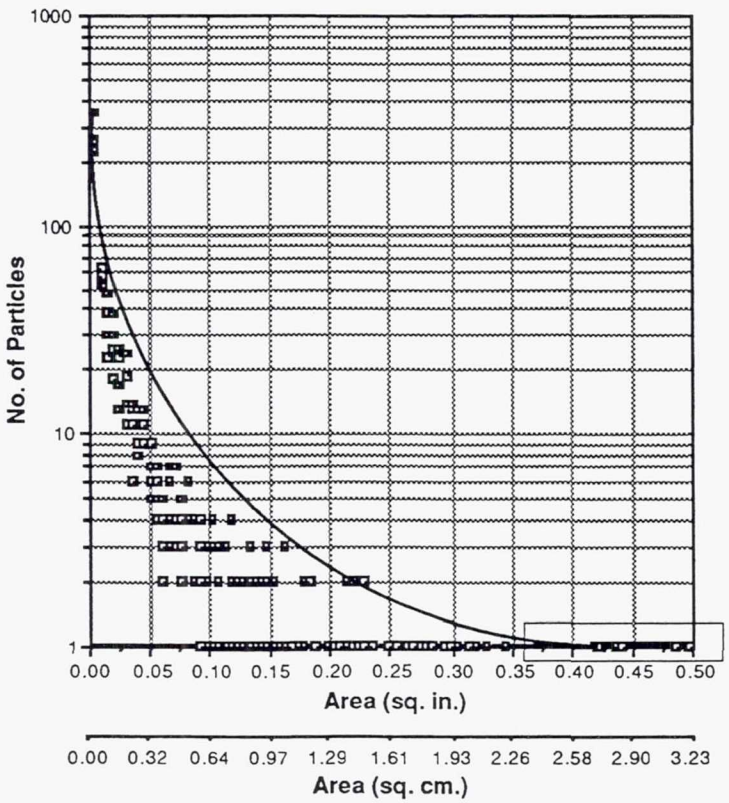

Figure 15. Shed Ice Particle Distribution With Upper Bound Curve

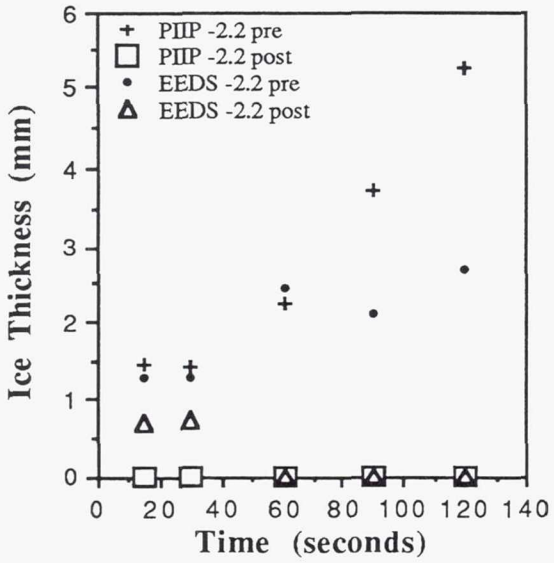

Figure 16. Measured Ice Thickness at the Leading Edge at mid-span for -2.2 °C, 0.70 g/m^3 LWC, 103 m/s airspeed. PIIP was at low pressure setting, and EEDS was at mid-power setting.

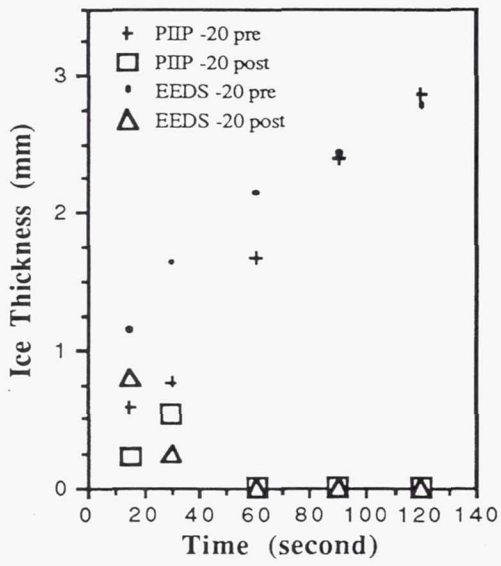

Figure 17. Measured Ice Thickness at the Leading Edge at mid-span for -20 °C, 0.38 g/m^3 LWC, 103 m/s airspeed. PIIP was at low pressure setting, and EEDS was at mid-power setting.

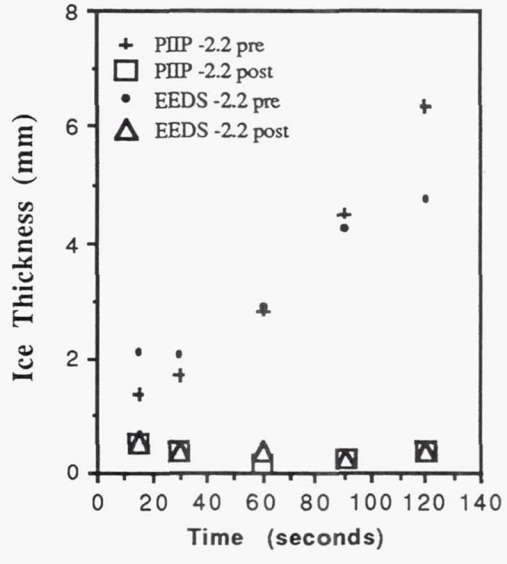

Figure 18. Measured Ice Thickness at the Lower Surface at mid-span for -2.2 °C, 0.70 g/m^3 LWC, 103 m/s airspeed. PIIP was at low pressure setting, and EEDS was at mid-power setting.

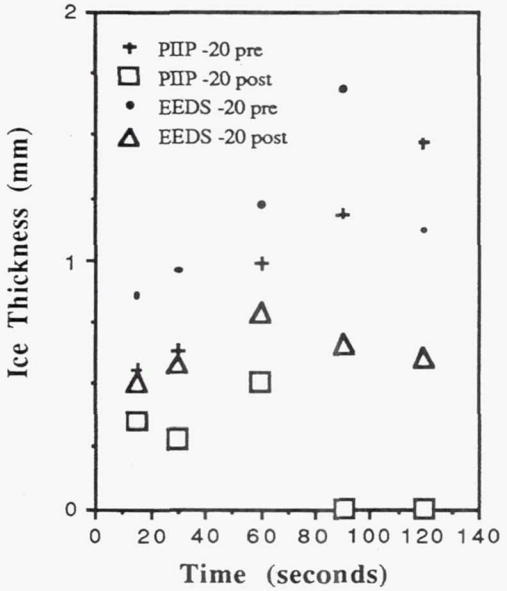

Figure 19. Measured Ice Thickness at the Lower Surface at mid-span for -20 °C, 0.38 g/m^3 LWC, 103 m/s airspeed. PIIP was at low pressure setting, and EEDS was at mid-power setting.

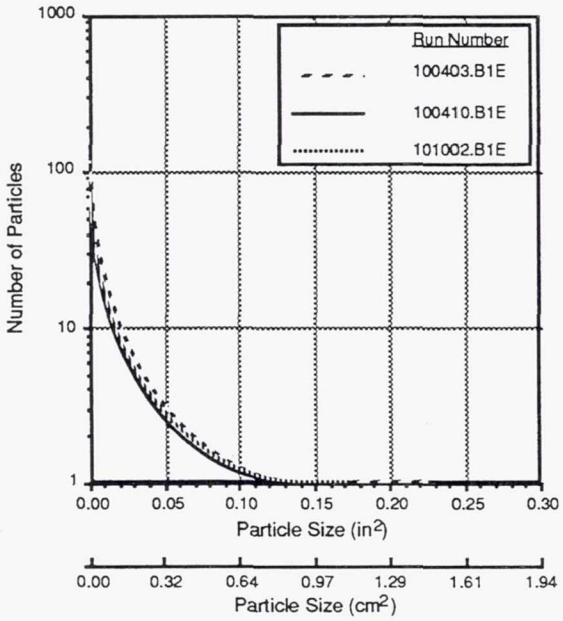

Figure 20. Shed Ice Size Distribution - Data Repeatability (PIIP, -2.2° C, 60 sec firing cycle, mid-span)

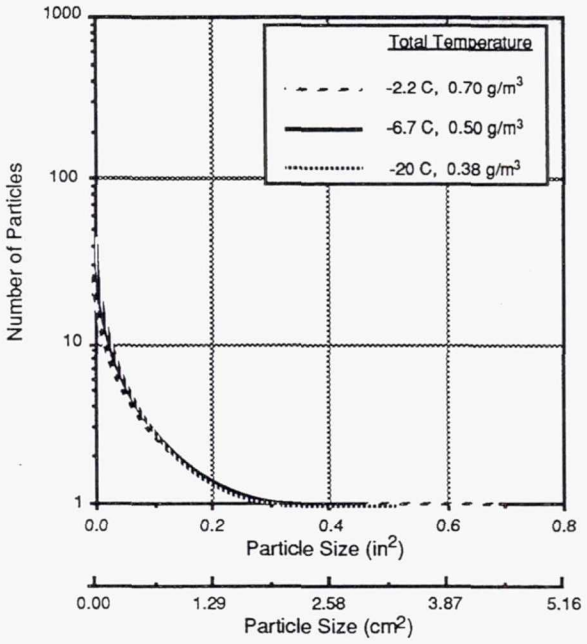

Figure 21. Shed Ice Size Distribution - Temperature/LWC Effects (EEDS, 60 sec firing cycle, mid-span)

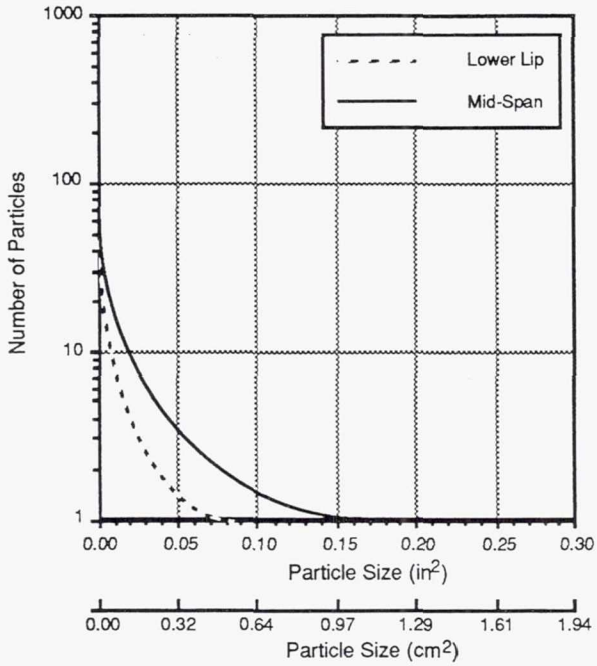

Figure 22. Shed Ice Size Distribution - Geometry Effects (PIIP, -20° C, 60 sec firing cycle)

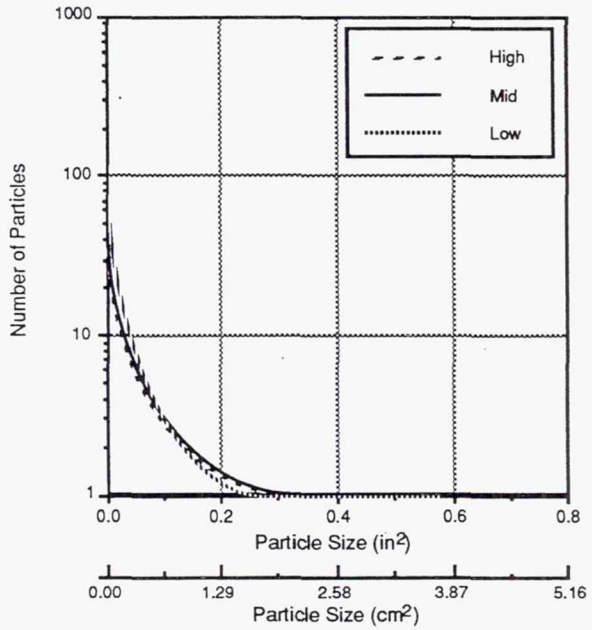

Figure 23. Shed Ice Size Distribution - Energy Effects (EEDS, -20° C, 60 sec firing cycle, mid-span)

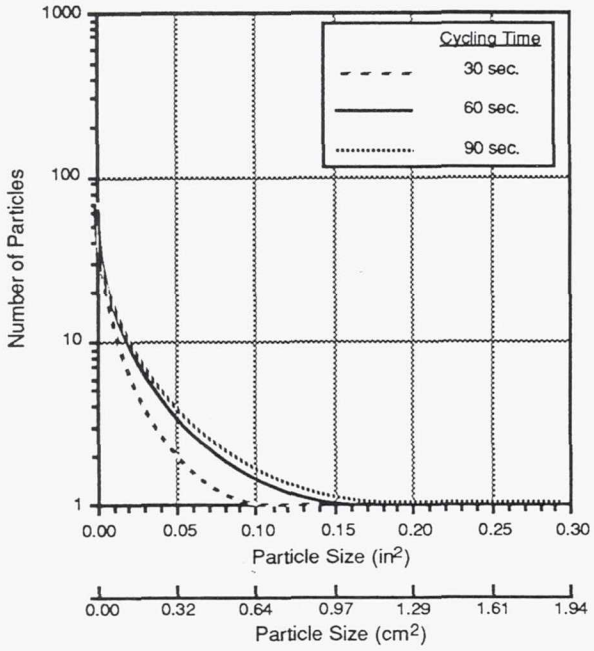

Figure 24. Shed Ice Size Distribution - Cycling Time Effects (PIIP, -20° C, mid-span)

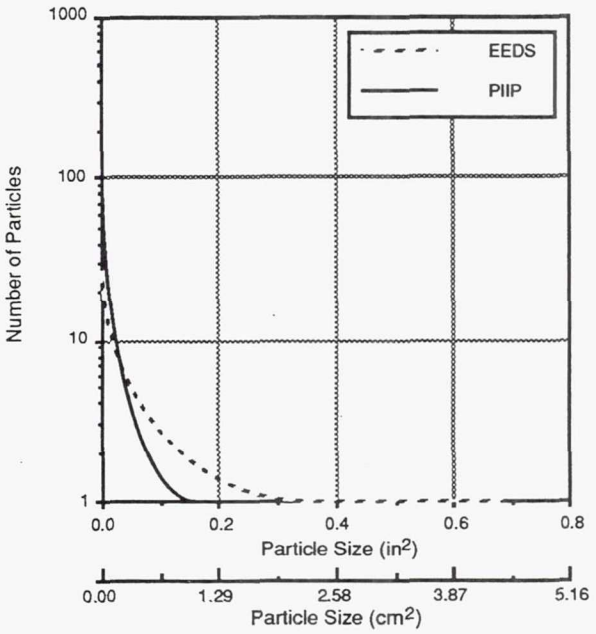

Figure 25. Shed Ice Size Distribution - System Comparison (-2.2° C, 60 sec firing cycle, mid-span)

REPORT DOCUMENTATION PAGE

Form Approved
OMB No. 0704-0188

1. AGENCY USE ONLY (*Leave blank*)	2. REPORT DATE	3. REPORT TYPE AND DATES COVERED
	January 1993	Technical Memorandum

4. TITLE AND SUBTITLE

Results of Low Power Deicer Tests on a Swept Inlet Component in the NASA Lewis Icing Research Tunnel

5. FUNDING NUMBERS

WU–505–68–10

6. AUTHOR(S)

Thomas H. Bond and Jaiwon Shin

7. PERFORMING ORGANIZATION NAME(S) AND ADDRESS(ES)

National Aeronautics and Space Administration
Lewis Research Center
Cleveland, Ohio 44135–3191

8. PERFORMING ORGANIZATION REPORT NUMBER

E–7495

9. SPONSORING/MONITORING AGENCY NAMES(S) AND ADDRESS(ES)

National Aeronautics and Space Administration
Washington, D.C. 20546–0001

10. SPONSORING/MONITORING AGENCY REPORT NUMBER

NASA TM–105968
AIAA–93–0032

11. SUPPLEMENTARY NOTES

Prepared for the 31st Aerospace Sciences Meeting & Exhibit sponsored by the American Institute of Aeronautics and Astronautics, Reno, Nevada, January 11–14, 1993. Thomas H. Bond and Jaiwon Shin, NASA Lewis Research Center. Responsible person, Thomas H. Bond, (216) 433–3414.

12a. DISTRIBUTION/AVAILABILITY STATEMENT

Unclassified - Unlimited
Subject Categories 02 and 07

12b. DISTRIBUTION CODE

13. ABSTRACT (*Maximum 200 words*)

Tests were conducted under a USAF/NASA Low Power Deicer program on two expulsive technologies to examine system performance on hardware representative of a modern aircraft part. The BF Goodrich Electro-Expulsive Deicing System and Pneumatic Impulse Ice Protection System were installed on a swept, compound curve, engine inlet component with varying leading edge radius, and tested through a range of icing and system operating conditions in the NASA Lewis Icing Research Tunnel. A description of the experimental procedure and results, including residual ice thickness, shed ice particle size, and changes in system energy/pressure characteristics are presented here.

14. SUBJECT TERMS

Deicing systems; Shed ice particle size

15. NUMBER OF PAGES

20

16. PRICE CODE

A03

17. SECURITY CLASSIFICATION OF REPORT	18. SECURITY CLASSIFICATION OF THIS PAGE	19. SECURITY CLASSIFICATION OF ABSTRACT	20. LIMITATION OF ABSTRACT
Unclassified	Unclassified	Unclassified	

National Aeronautics and
Space Administration

Lewis Research Center
Cleveland, Ohio 44135